Optical study of competition between ordering and metallicity in $La_{2-2x}Sr_{1+2x}Mn_2O_7$

J. Kunze,[1] S. Naler,[1] J. Bäckström,[1] M. Rübhausen,[1] and J. F. Mitchell[2]
[1]*Institut für Angewandte Physik, Universität Hamburg, Jungiusstraße 9, D-20355 Hamburg, Germany*
[2]*Materials Science Division, Argonne National Laboratory, Argonne, Illinois 60439*
(Received 14 August 2002; revised manuscript received 6 February 2003; published 15 April 2003)

We study by spectroscopic ellipsometry the optical in-plane anisotropies in $La_{2-2x}Sr_{1+2x}Mn_2O_7$ with $0.32 \leqslant x \leqslant 0.40$ above and below the metal to insulator (MI) transition. Spectral-weight changes in the optical conductivity occur at a cross-over temperature $T' = 280$ K for all dopings. Local ordering of orbital and charge degrees of freedom sets in doping dependently at temperatures of 145 K$\leqslant T^* \leqslant$310 K. Below the MI transition we observe for all dopings except $x = 0.36$ a vanishing of the charge ordering and an isotropic and metallic state at low frequencies, whereas the local orbital ordering persists. For $x = 0.36$ we observe two different characteristic developments of the ordering processes, one being compatible with the parabolic doping dependence on T^* established by the other doping levels and the second showing ordering at a temperature slightly above the MI transition. We argue that our observations are compatible with a phase separation scenario.

DOI: 10.1103/PhysRevB.67.134417 PACS number(s): 78.20.−e, 75.30.−m, 75.40.−s

The microscopic phase separation occuring in strongly correlated perovskites has been invoked to explain many peculiar phenomena, such as the pseudogap state in cuprates or the proximity between metallic and charge-ordered states in manganites.[1–7] Moreover, the question of how lowered dimensionality, yielding a predominantly two-dimensional (2D) system, influences the interplay between local ordering phenomena and global ground-state properties, is of crucial importance to understand the competition or coexistence between states with different magnetic and electronic characteristics.[1–3]

$La_{2-2x}Sr_{1+2x}Mn_2O_7$ (LSMO327) is the naturally layered $n=2$ member of the Ruddelsden-Popper series $(La,Sr)_{n+1}Mn_nO_{3n+1}$.[8] Like its cubic perovskite $n=\infty$ relative, it can exhibit the colossal magnetoresistance effect, a magnetic-field induced transition to a metallic state. Due to the 2D nature of LSMO327, the 3D ferromagnetic ordering is weaker; therefore, the metal-to-insulator transition temperature T_{MI} is reduced to 106–131 K and the in-plane conductivity differs by 2–4 orders of magnitude compared to the out-of-plane conductivity.[9,10] Within the paramagnetic range, evidence for a residual reduced ferromagnetism has been measured.[11] Moreover, striped features have been predicted from an orbital-degenerate double exchange model above T_{MI}.[12]

The anisotropies of the optical properties of a material can provide information on ordering phenomena on different length scales.[13–16] As different spectral regions can be attributed to distinct optical processes a determination of the source of the related ordering process is possible.[17,18] Spectroscopic ellipsometry measures relative amplitude and phase changes of light reflected from a sample and, thus, does not require the mandatory Kramers-Kronig analyses of reflectometry studies. This technique allows very accurate measurements of the complex dielectric function and its anisotropies.[19–21] As has been shown recently in pseudocubic manganites, detailed information on the temperature evolution of the optical anisotropies of charge and orbital ordering are valuable to understand the cooperative coupling between the different degrees of freedom.[13–15]

Here we report on a spectroscopic ellipsometry study of the in-plane anisotropic dielectric function of LSMO327 with $0.32 \leqslant x \leqslant 0.40$ covering the midinfrared to deep ultraviolet spectral range at temperatures between 25 and 475 K. The temperature evolution of the dielectric function can be described in essentially three steps. First, we find a cross-over temperature in the spectral weight development at doping independent value of $T' = 280$ K. Second, we find in the insulating phase below a crossover temperature T^* between 145- and 310-K optical anisotropies, that are doping dependent, in the high- and low-energy regions, evidencing orbital and charge ordering, respectively. The doping dependence of T^* shows a parabolalike shape similar to T_{MI}. Third, below $T_{MI} \approx 125$ K, we find a suppression of the charge ordering and a development of a long-range metallic state. Remarkably, the short-range orbital anisotropy that was clamped to the onset of charge ordering persists in the metallic state and indicates remaining local orbital order. Our results support the phase separation scenario in layered manganites.[7]

We have performed our experiments with the extended Sentech SE850 that covers a spectral range from 0.48 to 5.6 eV by using a Fourier-transform spectrometer below 1.5 eV and a grating spectrometer above 1.4 eV. The basic experimental configuration is shown in Fig. 1. The LSMO327

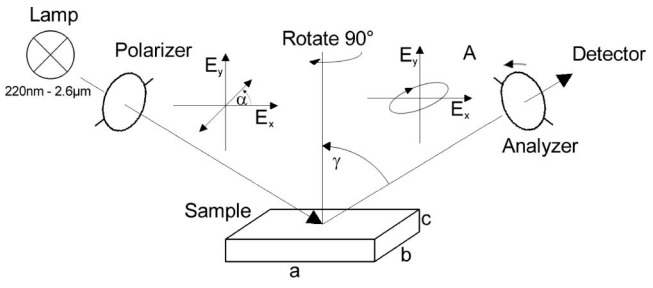

FIG. 1. Experimental setup. Ellipsometry measures in reflection the polarization ellipse from incident linearly or circularly polarized light. The sample is turned by 90° around the *c* axis, yielding the ''ca'' and ''cb'' spectra, respectively, in order to obtain anisotropy information.

single crystals with $0.32 \leqslant x \leqslant 0.40$ used for this study were synthesized as described elsewhere.[8] They have been well characterized in the literature and show a T_{MI} developing from 106 K at $x=0.32$ to 131 K for $x=0.36$ and 115 K for $x=0.40$.[8,9,11,22–26] The samples were cleaved out of the as-grown crystal boules yielding monocrystalline mirrorlike ab plane surfaces without polishing. The crystals $x=0.36$-ii and 0.38 have been cleaved directly prior to measurement in order to rule out the influence of surface degradation and contamination. The samples were mounted on pieces of sand-blasted silicon and placed in an ultra-high vacuum cryostat. The windows show no measurable depolarization effects due to their stress-free mounting. Typical base pressures at room temperature were 3×10^{-8} mbar. The differentially pumped revolvable cryostat holds a reference sample simultaneously with a crystal in order to check for freezeout or other artifacts. The reference sample is a 400 nm SiO_2 layer on bulk Si. The measured amplitude and phase changes were converted into the dielectric function $\epsilon = \epsilon_1 + i\,\epsilon_2$ by using the model for an isotropic semi-infinite material.[19] This assumption is well justified as the observed optical anisotropies in the energy range from 0.48 to 5.6 eV are generally weak compared to the overall signal.

Figure 2 shows the optical conductivity $\sigma = \epsilon_0 \epsilon_2 \omega$ for LSMO327 with $0.32 \leqslant x \leqslant 0.40$ at four temperatures. All samples show basically the same trends with temperature and only a small variation with doping. For clarity we have split the spectral range into three regions of interest. We call the spectral range between 0.5 and 0.8 eV the ''free charge carrier'' region, because it is mostly sensitive to the existence or absence of a Drude reponse at $\omega=0$. The energy range between 0.8 and 2.2 eV is denoted the ''bound charge carrier'' region, as it reflects mainly the existence of trapped charges and is sensitive to charge ordering.[13] Finally, we label the energy region larger than 3.5 eV as the ''orbital'' region. It is dominated by optical transitions between the O-$2p$ and Mn-e_g levels and, thus, should be very sensitive to specific orbital configurations and ordering.[13,15,18] Figure 2 shows a constant increase of spectral weight in the ''free charge carrier'' region with decreasing temperature that becomes strongly promoted when the sample enters the metallic state. The small enhancement of the spectral weight above T_{MI} is clearly related to the shifting of the ''bound charge carrier'' peak towards lower energies. This peak vanishes as the charges are released in the metallic state and form the Drude response. The orbital spectral region shows no temperature dependence when cooling from 425 K down to 300 K, but below 300 K develops a clear decrease of spectral weight.

Figures 3(a)–3(c) show the integrated spectral weight of the three spectral regions indicated in Fig. 2. The data have been normalized to correct for the slight overall offset due to different doping. In Fig. 3(d) we show the integral over the complete measured spectral range. Overall, the temperature dependence shows striking similarities among the different samples. Indeed, we find for all samples in the ''free charge carrier'' region in Fig. 3(a) a continuous increase of the spectral weight that develops a distinct anomaly at the metal-insulator (MI) transition. Even more drastic are the changes

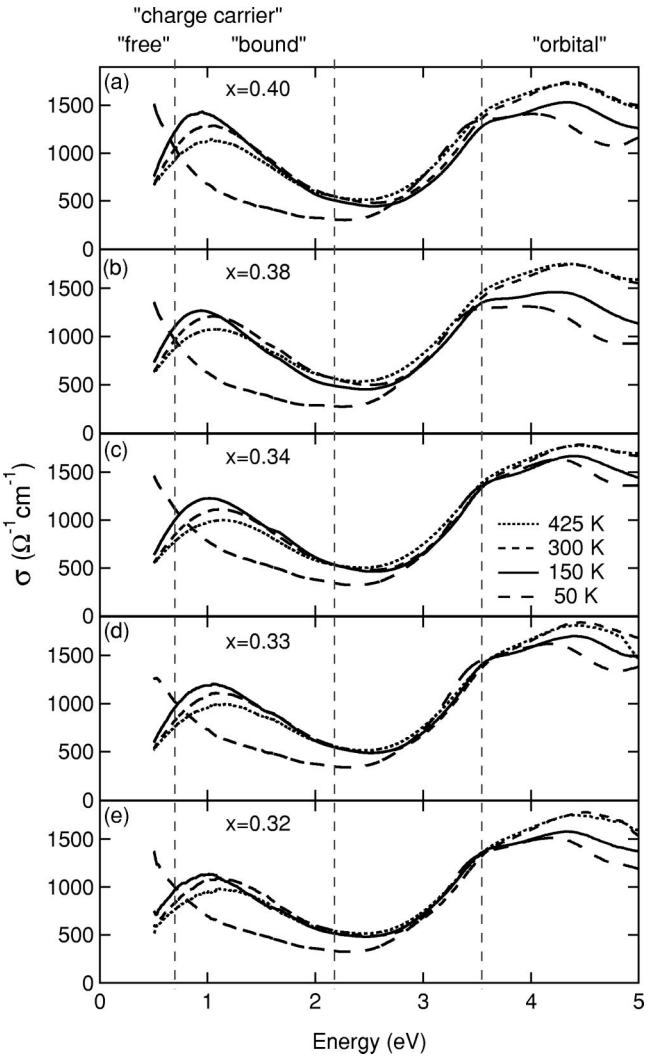

FIG. 2. Optical conductivity of LSMO327 with different doping levels at different temperatures as indicated. The spectral ranges, named ''free'' and ''bound charge carriers'' as well as ''orbital'' are marked.

in the ''bound charge carrier'' region in Fig. 3(b). It shows a linear increase of roughly 10% with decreasing temperature from 475 to 300 K, and saturates in a temperature range between 280 and 130 K. In the metallic state below 130 K the ''bound charge carrier'' region dramatically loses spectral weight and saturates at roughly 50% of its maximum value. Figure 3(c) displays the temperature evolution of the spectral weight in the ''orbital'' region. It is constant down to roughly 280 K, where a first drop occurs. This loss continues deep into the metallic state. Figure 3(a)–3(c) establish the existence of two characteristic temperatures, one of which is clearly connected to the MI transition at $\approx$130 K and the other to an additional effect developing around 280 K. We label this second crossover temperature T'. The integrated spectral weight in Fig. 3(d) shows that, especially below T_{MI}, spectral weight is lost to the Drude peak, which is to a large extent located outside our frequency range. There seems to be an additional shift of spectral weight at 280 K, i.e., T', to an energy region that is not directly accessed by

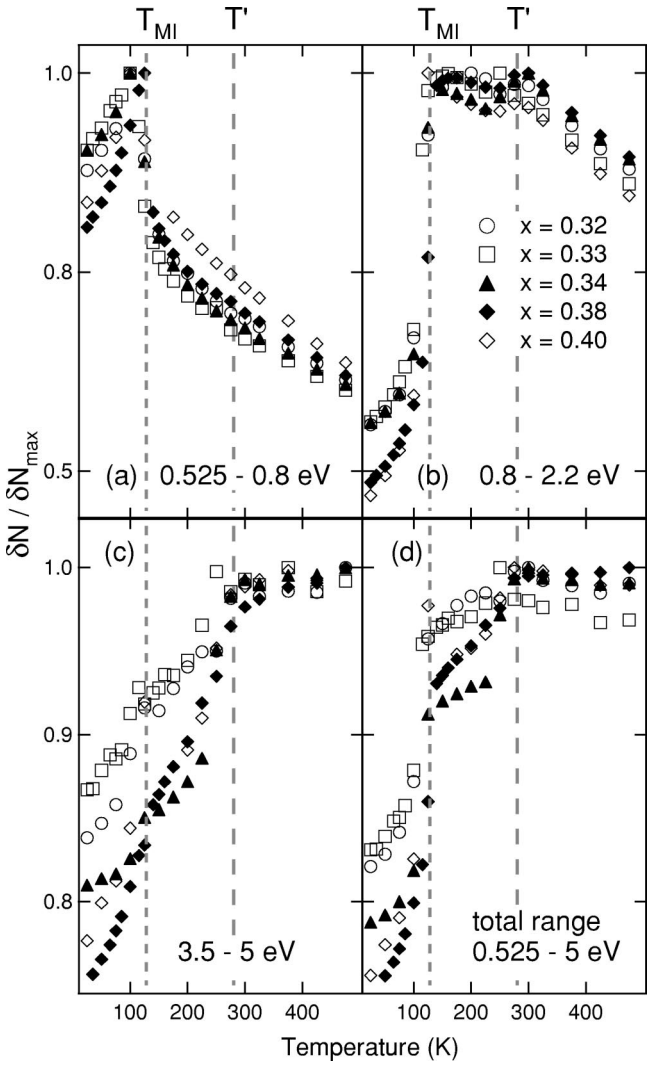

FIG. 3. Normalized integrated optical conductivity changes for four different spectral ranges corresponding to the ''free'' (a) and ''bound charge carrier'' (b) as well as ''orbital'' (c) spectral ranges. In (d) we show the integrated spectral weight over the total measured spectral range.

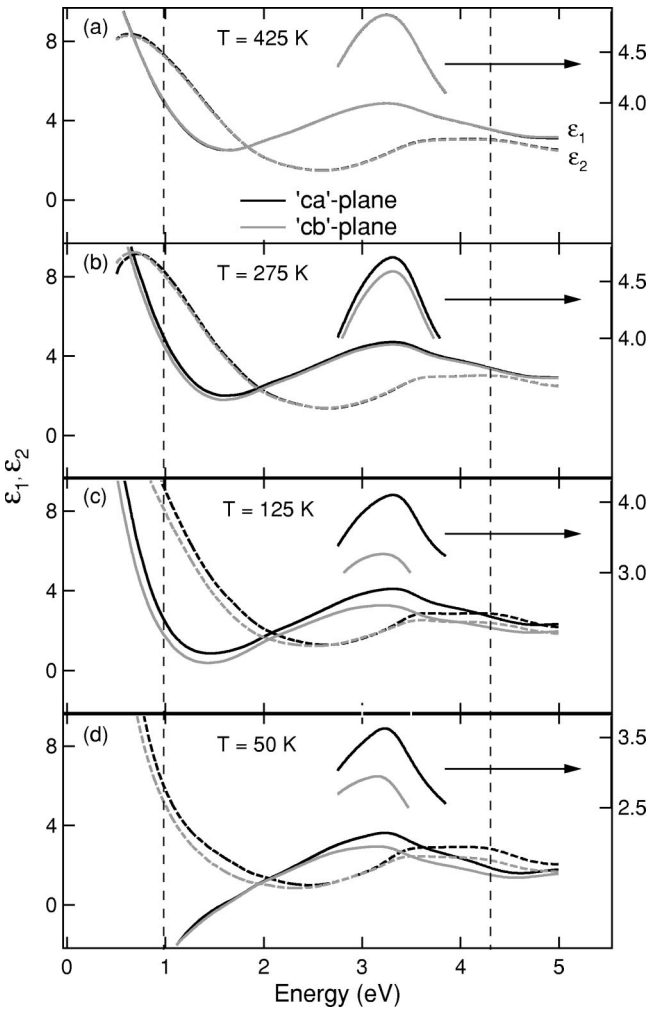

FIG. 4. Evolution of the optical anisotropy in the complex dielectric function ($x=0.34$). ϵ_1 and ϵ_2 are denoted by solid and dashed lines, whereas the two 90° rotated dielectric functions denoted as ''ca'' and ''cb'' are represented by black and gray lines, respectively. The insets display ϵ_1 on an expanded scale. The dashed vertical lines show the points choosen for evaluation of Δ^{ϵ_1}.

our measured range. On the other hand, the constant value of the integral over the total energy range above T' shows that the gain of spectral weight in the low-energy ranges [Figs. 3(a) and 3(b)] in this temperature region is balanced by a redistribution towards higher energies within the measured spectral range. The observed $T' \approx 280$ K coincidences with a reported step in the in-plane magnetization for the $x=0.40$ sample.[26]

To obtain additional information about the observed anomalies we have investigated the development of optical anisotropies. They can occur if local properties have on the typical length scale of the light a preferred orientation. The emergence of a preferred orientation is ordering. Thus, such anisotropies can indicate the existence of orbital or charge ordering. For this purpose we measured the dielectric function in two in-plane configurations that are 90° rotated to each other around the c axis (see Fig. 1). The planes of incidence of these two measurements are denoted as ''ca'' and ''cb.'' We point out that optical anisotropies measured this way evidence orderings even in the case of multidomain structures, since a prerequisite for optical anisotropy on an averaged scale is that the individual domains are anisotropic. However, if a multidomain structure occurs, the magnitude of the observed optical anisotropy of the average structure will be lower than for a single domain sample.

Figure 4(a) shows the completely isotropic high-temperature dielectric function. Even the enlarged plot of ϵ_1 in the spectral range around 3.5 eV shows no signs of optical anisotropy. This situation changes at 275 K [see Fig. 4 (b)]. Here we clearly see the simultaneous appearance of optical anisotropies in ϵ_1 and ϵ_2, both, in the ''bound charge carrier'' region around 1 eV and in the ''orbital'' region around 4 eV. These anisotropies are further enhanced at lower temperatures. It should be noted that both the increased volume fraction of the ordered phase and increased correlation lengths can result in increased anisotropy. Moreover, from the simultaneous appearance of anisotropy at 0.5 and at 4.25

eV we conclude that the growth of ordered domains in LSMO327 is significantly faster than, e.g., in $Bi_{0.8}Ca_{0.2}MnO_3$, where the optical anisotropy develops over a wider temperature range from short to long wavelengths.[13] At 125 K, slightly above the MI transition, the data strongly resemble those of charge and orbital ordered $Bi_{0.8}Ca_{0.2}MnO_3$, displaying large anisotropies around 1 and 3.5 eV in ϵ_1.[13] Based on this analogy, we associate T^* with the onset of charge and orbital order in LSMO327. However, close to the plasma frequency in the 50-K data in Fig. 4(d), representing the ''Drude'' contribution, ϵ_1 displays an isotropic behavior, whereas the the same pair of spectra shows large anisotropies around 3.5 eV. In the following we focus on ϵ_1, as it gives a direct measure of the optical anisotropies related to charge and orbital degrees of freedom.[13] ϵ_1 and ϵ_2 are Kramers-Kronig related, implying that spectral features will not appear at exactly the same frequency in both quantities. As an example, at 1 eV ϵ_1 is dominated by the plasma response and represents the metallicity (i.e., free charges), whereas ϵ_2 represents an overlap between the Drude tail and contributions coming from inter-band processes. When measuring at finite frequencies, the best way of obtaining information about the free carriers is to analyze ϵ_1 rather than ϵ_2. We evaluate $\Delta^{\epsilon_1}=|\epsilon_{1,ca}-\epsilon_{1,cb}|/\sqrt{\epsilon_{1,ca}^2+\epsilon_{1,cb}^2}$ shown in Figs. 5(a) and 5(b) for the charge and orbital channels at 1.05 and 4.25 eV, respectively. This parameter accurately reflects charge and orbital ordering even in a multidomain crystal.[13,14]

In Fig. 5(a) we show the evolution of optical anisotropy in the charge channel between the MI transition temperature T_{MI} and the anisotropy onset temperature T^* for all dopings. Figure 5(b) shows the development of an optical anisotropy in the orbital channel. T^* derived from the orbital channel equals T^* derived from the charge channel for all samples with the exception of the $x=0.40$ sample, whose onset of anisotropy is significant only in the charge channel. Remarkably, the anisotropy clearly persists below T_{MI} only in the orbital channel whereas it vanishes in the charge channel, i.e., close to the plasma frequency, when entering the metallic state. T^* is 200 K for the $x=0.32$ sample, develops to 290 K for $x=0.34$ and 0.38, where it is also close to T' as clarified in Fig. 3, and to 200 K for $x=0.40$.

Our results show that even though the orbital anisotropy appears at the same temperature as the charge anisotropy, it seems to be unaffected by the MI transition. This suggests that locally orbital ordered clusters develop and persist relatively unchanged in the metallic state. This idea is not in disagreement with the observed long-range metallicity, because the low-frequency part of the data will most likely be affected by the global properties of the sample.[27] Above T_{MI} quasistatic Jahn-Teller distortions are reported from neutron and x-ray scattering studies.[28,29] This connects very well to our observation of charge and orbital ordering between T_{MI} and T^*. But our results demonstrate, that the vanishing of those Jahn-Teller distortions below T_{MI} does not imply the vanishing of the orbital order. However, it does contrast with the observation at T^* that orbital and charge orderings seem to be clamped to each other, has also been observed for

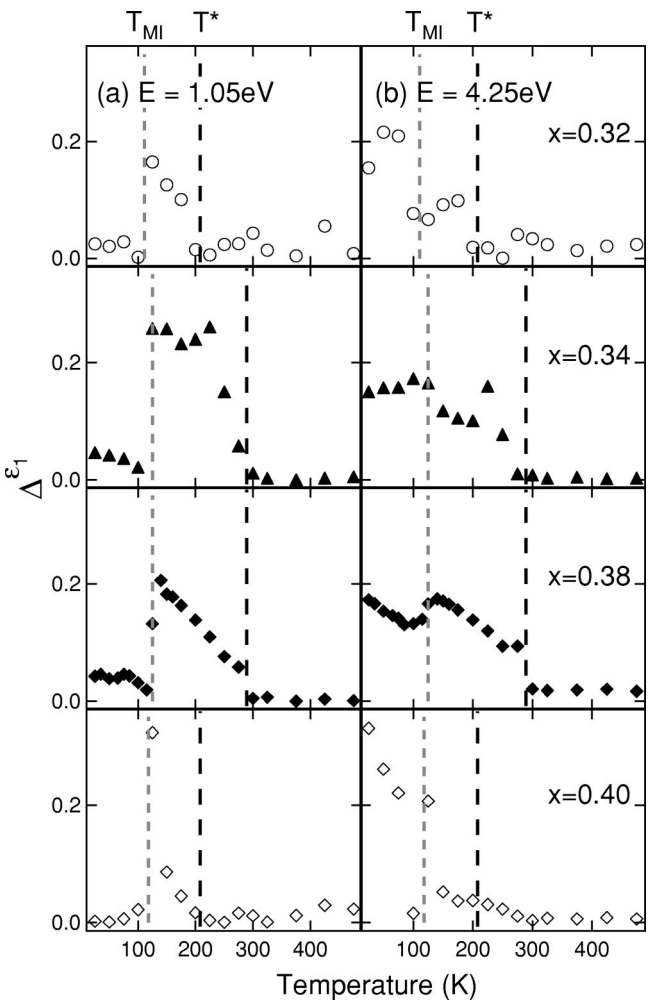

FIG. 5. Evolution of the order parameter Δ^{ϵ_1} representing the optical anisotropies in the charge at 1.05 eV (a) and in the orbital channels at 4.25 eV (b). T^* for different dopings as indicated. The 100-K anomaly in (b) for $x=0.40$ is the result of a sign reversal in $\epsilon_{1,ca}-\epsilon_{1,cb}$.

$Bi_{0.8}Ca_{0.2}MnO_3$ in the charge-ordered state.[13] The most plausible explanation for these observations would be a phase-separation scenario, where local degrees of freedom related to short-range charge and orbital ordering and global properties such as the development of a Fermi liquid become separated at T_{MI}.[30,31] This could be also viewed as a transition from a charge-ordered smectic structure melting into a metallic nematic phase below T_{MI}.[32] In the latter the anisotropy would be controlled by the parameter $v_f q$. Hence, the anisotropy vanishes in the long wavelength limit but remains finite on a local scale.[32]

Since Fig. 5 depicts a T^* value rising from $x=0.32$ through $x=0.34$ and from $x=0.40$ through $x=0.38$, the highest T^* value should be expected close to $x=0.36$ at a temperature above 290 K, connecting to the maximum T_{MI} value at this specific doping. However, the investigated $x=0.36$ samples showed a peculiar behavior that deserves further discussion. In Fig. 6 we compare ϵ_1 of two different $x=0.36$ sample surfaces taken from the same sample. The surface 0.36-i is the original surface cleaved out of the as-

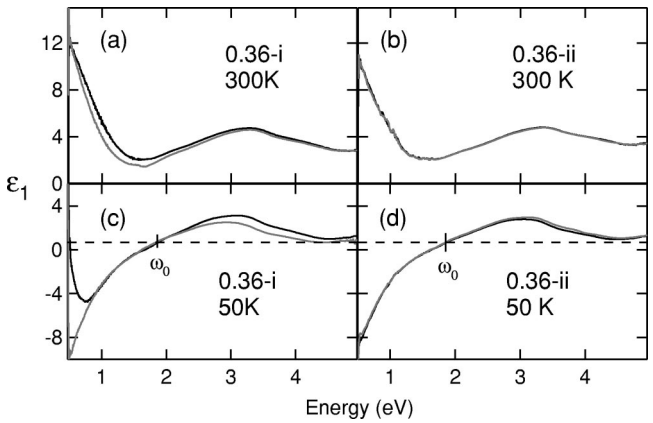

FIG. 6. Comparison of the "ca" and "cb" dielectric functions ϵ_1 of two different $x=0.36$ surfaces (0.36-i and 0.36-ii) of the same sample.

grown crystal boule and the 0.36-ii surface has been cleaved off the same sample just prior to the mesurements. In Fig. 6(b) the original 0.36-i surface shows an anisotropy already at 310 K. It evolves down to the MI transition and vanishes below the MI transition in the energy range around the

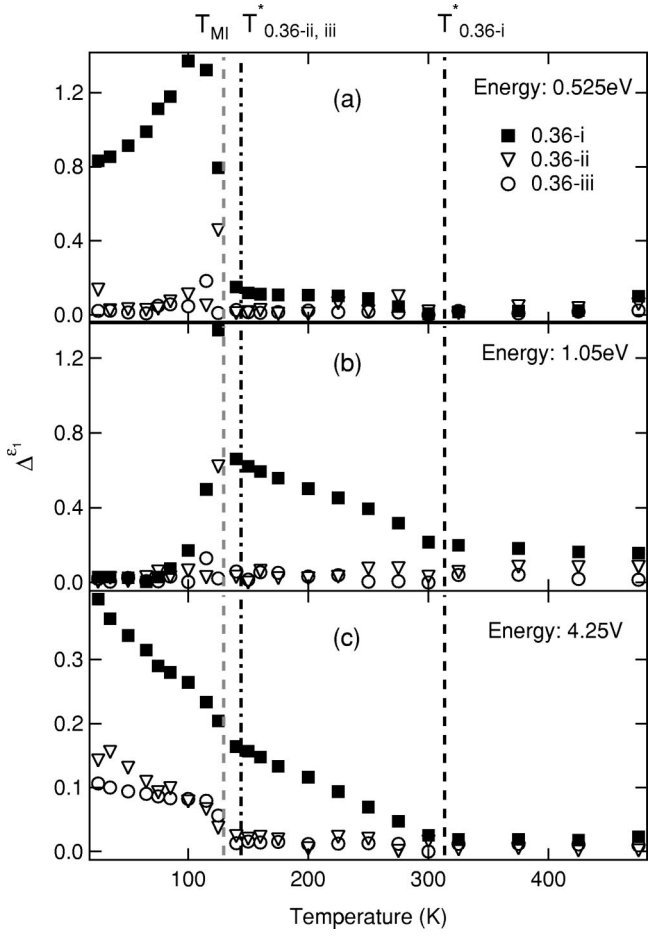

FIG. 7. Comparison of the optical anisotropy parameter of different $x=0.36$ sample surfaces at different energies: 0.36-i and 0.36-ii belong to the same samples, and 0.36-iii to a different sample.

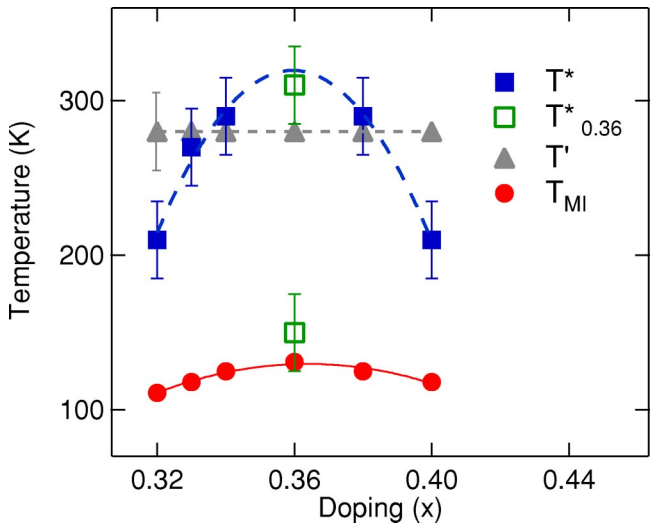

FIG. 8. The onset temperature of optical anisotropy T^*, optical conductivity spectral weight cross-over temperature T', and the metal to insulator temperature T_{MI} vs doping.

plasma frequency ω_0. But in contrast to all samples discussed before, a strong anisotropy in ϵ_1 opens up below 0.8 eV forming a second crossing of ϵ_1 and the zero line at roughly 0.5 eV in only one measured direction (see Fig. 6). This indicates the existence of an additional bound state in the mid to far infrared range weakening free charge motion in one but not the other direction. In contrast, in Fig. 6(b) the cleaved surface shows no anisotropy in ϵ_1 at 300 K. At temperatures below the MI transition, the charge channel anisotropy vanishes and the orbital channel anisotropy persists as seen in Fig. 6(c). This behavior is similar to the the data shown in Fig. 5.

In addition to these two surfaces, we measured the 0.36-iii surface of a different sample that was not freshly recleaved. This original surface exhibits a behavior that is similar to the freshly cleaved 0.36-ii surface. Thus the effect measured on the 0.36-i surface does not result from surface degradation.

For a better understanding, we compare in Fig. 7 the temperature dependent anisotropy of the three $x=0.36$ sample surfaces. In order to cover the low-energy anisotropy Δ^{ϵ_1} observed at the 0.36-i surface, we also evaluated the anisotropy at 0.525 eV, as shown in Fig. 7(a). Besides from the 0.36-i surface, all other $x=0.36$ surfaces show no significant anisotropy in this low energy range. This means, that the 0.36-i surface is the only one that develops nanometer scale domains embedded in an unordered matrix, that connect to structures comparable to the wavelength of the incoming light, i.e., $\approx 1.5\mu$, providing the prerequesite to see a preferred orientation in the area probed by the spot, i.e., $\approx$ millimeters. Figure 7(b) shows the anisotropy at 1.05 eV. At this energy all surfaces show isotropy well below the MI transition in consistence with the other investigated dopings (Fig. 5). Above the MI transition up to 310 K only the 0.36-i surface has a significant anisotropy indicating charge ordering, whereas the 0.36-ii and 0.36-iii surfaces stay isotropic. In Fig. 7(c) the orbital anisotropy is present below the MI transition as it is for all other samples indicating orbital ordering below the MI transition. It decreases with increasing temperature until it vanishes at $T^*_{0.36\text{-ii, iii}}$ of 145 K for the

0.36-ii and 0.36-iii surfaces close to the MI transition and at $T^*_{0.36\text{-i}}$ of 310 K for the 0.36-i surface. Hence, for one and the same doping, we find two different T^* values. Overall, the 0.36-i surface behaves fundamentally different not only because of the higher T^* value but also because the charge ordering is reflected at a lower energy being developed in a presumably metallic state below 132 K. Interestingly, in the ''orbital'' range [see Fig. 7(c)] all three investigated surfaces show a similar sudden increase of anisotropy below the MI transition.

Figure 8 highlights the doping dependence of T^*, T', and T_{MI}. T^* exhibits a curved shape that is qualitatively similar to T_{MI}. The maximum T^* value being at $x=0.36$ connects well to the exposed role of this specific doping like the highest T_{MI} value and the lack of lattice anomalies at the MI transition.[24] In addition, the low T^* value found at the other $x=0.36$ surfaces puts this specific doping into our focus of interest.

It has been debated that short-range ordering in form of stripes might well be responsible for the pseudogap phase in the cuprates.[3,33,34] Results on layered manganites indicate that short-range charge and orbital ordering can be made responsible for an unconventional state preceding a MI transition at lower temperatures.

In conclusion, we have shown that LSMO327 exhibits three critical temperatures signaled by dramatic changes in the dielectric function. First, at $T' \approx 280$ K, a loss of spectral weight over the entire investigated spectral range (0.5–5 eV) is observed, and precedes the onset of the formation of an optically anisotropic state at T^* between 200 and 310 K depending on the doping level, signaling the onset of orbital and charge ordering. This onset temperature drops to 145 K for certain $x=0.36$ sample surfaces. Second, below the metal to insulator transition at around 125 K, we find a suppression of the charge ordering and the development of a long-range metallic state. However, the anisotropy in the orbital energy range ≈ 4.25 eV, that was clamped to the onset of charge ordering, persists in the metallic state indicating remaining local orbital order. Thus, our results support the phase separation scenario in layered manganites.

We acknowledge many stimulating discussions with U. Merkt, M.V. Klein, and S.L. Cooper and financial support through the DFG via Ru773/2-1.

[1] R. H. McKenzie, Science **278**, 820 (1997).
[2] A. P. Ramirez, J. Phys.: Condens. Matter **9**, 8171 (1997).
[3] V. J. Emery and S. A. Kivelson, Nature (London) **374**, 437 (1995).
[4] A. J. Millis, Nature (London) **392**, 438 (1998).
[5] A. J. Millis, B. I. Shraiman, and R. Mueller, Phys. Rev. Lett. **77**, 175 (1996).
[6] J. Burgy, M. Mayr, V. Martin-Mayor, A. Moreo, and E. Dagotto, Phys. Rev. Lett. **87**, 277202 (2001).
[7] E. Dagotto, T. Hotta, and A. Moreo, Phys. Rep. **344**, 1 (2001).
[8] J. F. Mitchell, D. N. Argyriou, J. D. Jorgensen, D. G. Hinks, C. D. Potter, and S. D. Bader, Phys. Rev. B **55**, 63 (1997).
[9] U. Welp, A. Berger, V. K. Vlasko-Vlasov, H. You, K. E. Gray, and J. F. Mitchell, J. Appl. Phys. **89**, 6612 (2001).
[10] T. Ishikawa, K. Tobe, T. Kimura, T. Katsufuji, and Y. Tokura, Phys. Rev. B **62**, 12 354 (2000).
[11] A. Berger, J. F. Mitchell, D. J. Miller, and S. D. Bader, J. Appl. Phys. **89**, 6851 (2001).
[12] T. Hotta, A. Feiguin, and E. Dagotto, Phys. Rev. Lett. **86**, 4922 (2001).
[13] M. Rübhausen, S. Yoon, S. L. Cooper, K. H. Kim, and S.-W. Cheong, Phys. Rev. B **62**, R4782 (2000).
[14] S. Yoon, M. Rübhausen, S. L. Cooper, K. H. Kim, and S.-W. Cheong, Phys. Rev. Lett. **85**, 3297 (2000).
[15] K. Tobe, T. Kimura, Y. Okimoto, and Y. Tokura, Phys. Rev. B **64**, 184421 (2001).
[16] Y. Okimoto, Y. Tomioka, Y. Onose, Y. Otsuka, and Y. Tokura, Phys. Rev. B **57**, 9377 (1998).
[17] H. L. Liu, S. L. Cooper, and S. W. Cheong, Phys. Rev. Lett. **81**, 4684 (1998).
[18] J. H. Jung, K. H. Kim, D. J. Eom, T. W. Noh, E. J. Choi, J. Yu, Y. S. Kwon, and Y. Chung, Phys. Rev. B **55**, 15 489 (1997).
[19] R. M. A. Azzam and N. M. Bashara, *Ellipsometry and Polarized Light* (North-Holland, Amsterdam, 1977).
[20] C. Presura, D. van der Marel, A. Damascelli, and R. K. Kremer, Phys. Rev. B **61**, 15 762 (1997).
[21] J. Kircher, Ph.D. thesis, Max-Planck-Institut für Festkörperforschung, Stuttgart, 1992.
[22] D. N. Argyriou, H. N. Bordallo, J. F. Mitchell, J. D. Jorgensen, and G. F. Strouse, Phys. Rev. B **60**, 6200 (1999).
[23] B. J. Campbell, R. Osborn, D. N. Argyriou, L. Vasiliu-Doloc, J. F. Mitchell, S. K. Sinha, U. Ruett, C. D. Ling, Z. Islam, and J. W. Lynn, Phys. Rev. B **65**, 014427 (2001).
[24] M. Medarde, J. F. Mitchell, J. E. Millburn, S. Short, and J. D. Jorgensen, Phys. Rev. Lett. **83**, 1223 (1999).
[25] D. B. Romero, Y. Moritomo, J. F. Mitchell, and H. D. Drew, Phys. Rev. B **63**, 132404 (2001).
[26] N. O. Moreno, P. G. Pagliuso, C. Rettori, J. S. Gardner, J. L. Sarrao, J. D. Thompson, D. L. Huber, A. Garcia-Flores, and S. B. Osero, Physica B **292**, 1 (2000).
[27] J. F. Mitchell, C. D. Ling, J. E. Millburn, D. N. Argyriou, A. Berger, and M. Medarde, J. Appl. Phys. **89**, 6618 (2001).
[28] L. Vasiliu-Doloc, S. Rosenkranz, R. Osborn, S. K. Sinha, J. W. Lynn, J. Mesot, O. H. Seeck, G. Preosti, A. J. Fedro, and J. F. Mitchell, Phys. Rev. Lett. **83**, 4393 (1999).
[29] D. N. Argyriou, J. W. Lynn, R. Osborn, B. Campbell, J. F. Mitchell, U. Ruett, H. N. Bordallo, A. Wildes, and C. D. Ling, Phys. Rev. Lett. **89**, 036401 (2002).
[30] X.-J. Fan, H. Koinuma, and T. Hasegawa, Phys. Rev. B **65**, 144401 (2002).
[31] M. Fäth, S. Freisem, A. A. Menovsky, Y. Tamioka, J. Aarts, and J. A. Mydosh, Science **285**, 1540 (1999).
[32] V. Oganesyan, S. A. Kivelson, and E. Fradkin, Phys. Rev. B **64**, 195109 (2001).
[33] T. Timusk and B. Statt, Rep. Prog. Phys. **62**, 61 (1999).
[34] I. Panas, A. Snis, and F. Bawa, J. Low Temp. Phys. **117**, 419 (1999).